International Journal of Nanomedicine

Dovepress
open access to scientific and medical research

Open Access Full Text Article

ORIGINAL RESEARCH

Biological and osseointegration capabilities of hierarchically (meso-/micro-/nano-scale) roughened zirconia

This article was published in the following Dove Press journal:
International Journal of Nanomedicine

Naser Mohammadzadeh Rezaei, Masakazu Hasegawa, Manabu Ishijima, Kourosh Nakhaei, Takahisa Okubo, Takashi Taniyama, Amirreza Ghassemi, Tania Tahsili, Wonhee Park, Makoto Hirota, Takahiro Ogawa

Weintraub Center for Reconstructive Biotechnology, Division of Advanced Prosthodontics, UCLA School of Dentistry, Los Angeles, CA, USA

Video abstract

Point your SmartPhone at the code above. If you have a QR code reader the video abstract will appear. Or use:

http://youtu.be/xLFkTfu0Jb8

Correspondence: Takahiro Ogawa
Weintraub Center for Reconstructive Biotechnology, Division of Advanced Prosthodontics, UCLA School of Dentistry, 10833 Le Conte Avenue (B3-081 CHS), Box 951668, Los Angeles, CA 90095-1668, USA
Tel +1 310 825 0727
Fax +1 310 825 6345
Email togawa@dentistry.ucla.edu

Purpose: Zirconia is a potential alternative to titanium for dental and orthopedic implants. Here we report the biological and bone integration capabilities of a new zirconia surface with distinct morphology at the meso-, micro-, and nano-scales.

Methods: Machine-smooth and roughened zirconia disks were prepared from yttria-stabilized tetragonal zirconia polycrystal (Y-TZP), with rough zirconia created by solid-state laser sculpting. Morphology of the surfaces was analyzed by three-dimensional imaging and profiling. Rat femur-derived bone marrow cells were cultured on zirconia disks. Zirconia implants were placed in rat femurs and the strength of osseointegration was evaluated by biomechanical push-in test.

Results: The rough zirconia surface was characterized by meso-scale (50 µm wide, 6–8 µm deep) grooves, micro-scale (1–10 µm wide, 0.1–3 µm deep) valleys, and nano-scale (10–400 nm wide, 10–300 nm high) nodules, whereas the machined surface was flat and uniform. The average roughness (Ra) of rough zirconia was five times greater than that of machined zirconia. The expression of bone-related genes such as collagen I, osteopontin, osteocalcin, and BMP-2 was 7–25 times upregulated in osteoblasts on rough zirconia at the early stage of culture. The number of attached cells and rate of proliferation were similar between machined and rough zirconia. The strength of osseointegration for rough zirconia was twice that of machined zirconia at weeks two and four of healing, with evidence of mineralized tissue persisting around rough zirconia implants as visualized by electron microscopy and elemental analysis.

Conclusion: This unique meso-/micro-/nano-scale rough zirconia showed a remarkable increase in osseointegration compared to machine-smooth zirconia associated with accelerated differentiation of osteoblasts. Cell attachment and proliferation were not compromised on rough zirconia unlike on rough titanium. This is the first report introducing a rough zirconia surface with distinct hierarchical morphology and providing an effective strategy to improve and develop zirconia implants.

Keywords: bone–implant integration, Y-TZP, hierarchical morphology, multi-scale rough, dental and orthopedic implant

Introduction

Titanium or titanium-alloy implants are widely used in orthopedic surgery and dentistry to reconstruct diseased and fractured bone and joints and to restore missing teeth. Clinical outcomes for titanium implants are acceptable, but a significant number of cases still require revision surgery after implant failure.[1–11] Implant therapy-related complications such as disability and long-lasting dependence caused by implant loosening remain significant,[11–13] and unfavorable anatomical and physiological states of the host bone can preclude implant therapy.[14–22] Further, the protracted healing time

required by implants to anchor into bone limits the application of implant therapy and reduces therapeutic benefit, particularly for dental implants. All these challenges are partially or largely attributable to the limited capability of implants to integrate with bone.

Current implant surfaces are roughened by various mechanical, physical, and chemical modification techniques such as sand-blasting, coating, acid-etching, and thermal processing.[23–28] There is good scientific evidence and a clinical consensus that roughened implants anchor better into bone than implants with relatively smooth surfaces.[23–31] This is not only due to the increased mechanical interlocking of bone and implants but also due to enhanced osteogenesis, improved quality of newly formed bone, and increased strength of interfacial molecular bonding.[30,32–34] In particular, there is a significant body of scientific evidence and long-term clinical outcome data supporting the efficacy of titanium implants with micro-scale roughness.[23–29,35] However, micro-roughened implants do not overcome all of the clinical problems noted above, and the development of roughened titanium surfaces seems to have reached a technical plateau such that the available rough titanium implants are equivalent in terms of their biological and bone integration capabilities. Creating an even more osteoconductive titanium implant has been a challenge.[36,37]

Zirconia appears to be a promising alternative to titanium for dental and orthopedic implants.[38–41] Although still at the initial market stage, implants made from yttria-stabilized tetragonal zirconia polycrystal (Y-TZP) are available as dental implants. Alumina-zirconia composite, or zirconia-toughened alumina (ZTA), has been used in orthopedic surgery. Zirconia may overcome some of the disadvantages of titanium such as allergic reactions and corrosion causing ion and debris release.[42–45] Further, zirconia may be bacteriaphobic[46–51] and, for dental implants, its similar color to tooth structures has an additional esthetic benefit over titanium, the grayish color of which can be visible through thin jaw bone and gingival tissues.[39,52]

There has been a considerable interest and effort in improving zirconia surfaces, particularly the development of surface roughening techniques. Physical,[53–55] chemical,[54–56] and thermochemical[57] modifications of zirconia surfaces successfully improved cellular response and function. However, roughness parameters reported for zirconia implants are generally lower than those for titanium implants.[54,58–62] As a result, the strength of bone–implant integration and the percentage of bone formation around implants are lower for zirconia than titanium implants.[39–41,55,59–61,63,64] Clinical studies also indicated that the success rate for zirconia implants is significantly lower than that for commonly used titanium implants.[39,59]

Here we have created a Y-TZP zirconia surface with distinct hierarchical surface morphology consisting of meso-, micro-, and nano-scale roughness. The objective of this study was to examine the biological and bone integration capabilities of this hierarchically roughened zirconia compared to relatively smooth machined zirconia.

Materials and methods

Zirconia samples and surface characterization

Zirconia experimental samples in disk (20 mm diameter, 1.5 mm thickness) and cylindrical form (1 mm diameter, 2 mm length) were machine-prepared from yttria-stabilized tetragonal zirconia polycrystal (Y-TZP) and assigned as the "machined surface" group. A rough zirconia surface was created by applying solid-state laser etching to engrave the machined zirconia samples. All samples were manufactured and provided by Nantoh Co., Ltd (Numazu, Japan) and sterilized by autoclaving before cell culture and animal studies. Surface morphology was examined by scanning electron microscopy (SEM; Nova 230 Nano SEM, FEI, Hillsboro, OR, USA) and an optical profile microscope (MeX, Alicona Imaging GmbH, Raaba, Graz, Austria) for three-dimensional imaging and profiling. The average roughness, root mean-square roughness, and peak-to-valley roughness were calculated. The chemical composition of the zirconia surfaces was evaluated by electron spectroscopy for chemical analysis (ESCA) using x-ray photoelectron spectroscopy (XPS) (Axis Ultra DLD, Kratos Analytical Ltd, Manchester, UK) under high-vacuum conditions (6×10^{-7} Pa). The hydrophilic or hydrophobic state of zirconia surfaces was evaluated by measuring the contact angle of 10 µL H_2O placed on the disks.

Osteoblast cell culture

Bone marrow-derived osteoblasts were isolated from the femurs of 8-week-old male Sprague–Dawley rats and placed into alpha-modified Eagle's medium supplemented with 15% fetal bovine serum, 50 µg/mL ascorbic acid, 10 mM Na-β-glycerophosphate, 10^{-8} M dexamethasone, and antibiotic–antimycotic solution containing 10,000 units/mL penicillin G sodium, 10,000 mg/mL streptomycin sulfate, and 25 mg/mL amphotericin B. Cells were incubated in a humidified atmosphere of 95% air and 5% CO_2 at 37°C. At 80% confluency, the cells were detached using 0.25% trypsin–1 mM EDTA-4Na and seeded onto zirconia disks placed in 12-well culture

dishes at a density of 3×10^4 cells/cm^2. The culture medium was renewed every three days.

Cell attachment and proliferation assays

The initial attachment of cells to zirconia surfaces was evaluated by measuring the number of cells attached to zirconia disks after 6 and 24 h of incubation. The density of propagated cells was quantified on day 3 of culture using a tetrazolium salt (WST-1)-based colorimetric assay (WST-1; Roche Applied Science, Penzberg, Germany). Each culture well was incubated at 37°C for 24 h with 100 µL WST-1 reagent. The amount of formazan produced was measured at 420 nm using an enzyme-linked immunosorbent assay (ELISA) reader (Synergy HT, BioTek Instruments, Winooski, VT, USA). The proliferative activity of cells was also measured by incorporating BrdU during DNA synthesis. On day 3 of culture, 100 µL of 100 mM BrdU solution (Roche Applied Science) was added to the culture wells followed by incubation for 10 h. After trypsinizing the cells and denaturing DNA, cultures were incubated with an anti-BrdU conjugated with peroxidase for 90 min and reacted with tetramethylbenzidine for color development. Absorbance was measured at 370 nm using an ELISA reader.

Morphology and spreading behavior of osteoblasts

Spreading behavior and cytoskeletal arrangement of osteoblasts seeded onto zirconia surfaces were examined using confocal laser scanning microscopy. At 6 and 24 h after seeding, cells were fixed in 10% formalin and stained using the fluorescent dye rhodamine phalloidin (actin filament, red color; Molecular Probes, Eugene, OR, USA). The area, perimeter, and Feret's diameter were quantified using an image analyzer (ImageJ, NIH, Bethesda, MD, USA).

Alkaline phosphatase (ALP) activity

Osteoblast ALP activity was examined on day 5 using image-based assays. Cultured cells were washed twice with Hanks' solution and then incubated with 120 mM Tris buffer (pH 8.4) containing 0.9 mM naphthol AS-MX phosphate and 1.8 mM fast red TR for 30 min at 37°C. The ALP-positive area was calculated as ([stained area/disk area) × 100])(%) using an image analyzer (ImageJ).

Real-time quantitative polymerase chain reaction (qPCR)

Gene expression was analyzed by qPCR on days 7 and 14. Total RNA was extracted from cells using TRIzol (Thermo Fisher Scientific, Waltham, MA, USA) and Direct-zol RNA MiniPrep kit (Zymo Research, Irvine, CA, USA). Extracted RNA was reverse-transcribed into first-strand cDNA using SuperScript III Reverse Transcriptase (Invitrogen). The quantitative PCR reaction was performed in a 20 µL volume containing 90 ng cDNA, 10 µL TaqMan Universal Master Mix II, and 1 µL TaqMan Gene Expression Assay using the QuantStudio 3 Real-Time PCR System (Thermo Fisher Scientific) to quantify expression of type I collagen, osteopontin, osteocalcin, and BMP-2 mRNA. GAPDH expression was used as the endogenous control.

Surgery

Eight-week-old male Sprague–Dawley rats were anesthetized by inhalation with 1%–2% isoflurane. After their legs were shaved and scrubbed with 10% povidone-iodine solution, the distal aspects of the left femurs were carefully exposed through skin incision and muscle dissection. The flat surfaces of the distal femurs were selected for implant placement. The implant site was prepared 11 mm from the distal edge of the femur by drilling with a 0.8 mm round burr and enlarged using reamers (#ISO 090 and 100). One cylindrical machined or roughened zirconia implant was placed into one femur, alternating the side on which each group of implants was placed. Surgical sites were then closed in layers. Muscle and skin were sutured separately with resorbable sutures. All of the experiments were performed following the protocol approved by The Chancellor's Animal Research Committee at the University of California at Los Angeles and followed the PHS Policy for the Humane Care and Use of Laboratory Animals and the UCLA Animal Care and Use Training Manual guidelines.

Implant biomechanical push-in test

The established implant biomechanical push-in test was used to assess the strength of bone–implant integration.[16,65] At weeks 2 and 4 of healing, femurs containing cylindrical implants were harvested and embedded into autopolymerizing resin with the top surface of the implant parallel to the ground. Micro-computed tomography was used to confirm that the implants were free from cortical bone support on the lateral and bottom sides of the implant. A testing machine (Instron 5544 electro-mechanical testing system, Instron, Canton, MA, USA) equipped with a 2,000 N load cell and a pushing rod (0.8 mm in diameter) was used to load the implant vertically downward at a crosshead speed of 1 mm/min. The push-in value was determined by measuring the peak of the load–displacement curve.

Morphological and elemental analyses of implant/tissue complex

After the push-in test at week 2 healing, all implants were carefully exposed and soaked in agitated water for one hour and dried under heat and vacuum. After being carbon sputter-coated, the specimens were examined by scanning electron microscopy (SEM). The elemental composition of the tissue remnants and the implant interface were analyzed by energy dispersive X-ray spectroscopy (EDX) (UltraDry EDS Detector and Noran System 6, Thermo Fisher Scientific).

Statistical analyses

Data on surface roughness parameters were collected from six sites on three different zirconia disks ($n = 6$). Three disks were used for all cell culture studies ($n = 3$) except for the analysis of cytomorphometry, where nine independent cells were evaluated ($n = 9$). Six animals were used for the biomechanical push-in test ($n = 6$) for each of the healing times. One-way ANOVA was performed to examine the difference between the machined and roughened zirconia groups. $p < 0.05$ was considered statistically significant.

Results

Creation of a hierarchical roughened morphology on zirconia

Low-magnification SEM of the surfaces of machined zirconia implants showed nearly no surface texture (350× image, Figure 1A). Higher magnification SEM depicted parallel linear traces from the machine turning with no other defined structures (5,000× and 20,000× images, Figure 1A). Laser-architected rough zirconia surfaces were characterized by parallel grooves formed at approximately 50 µm intervals, as shown by low-magnification SEM (350× and 1,000× images, Figure 1A). Grooves formed smooth curves with additional mild waviness within the curvature, as shown in 1,000× and 5,000× images of the surface (white dotted line in 1,000× and 5,000× images, Figure 1A). High-magnification images revealed the formation of nodular structures at the nano-scale

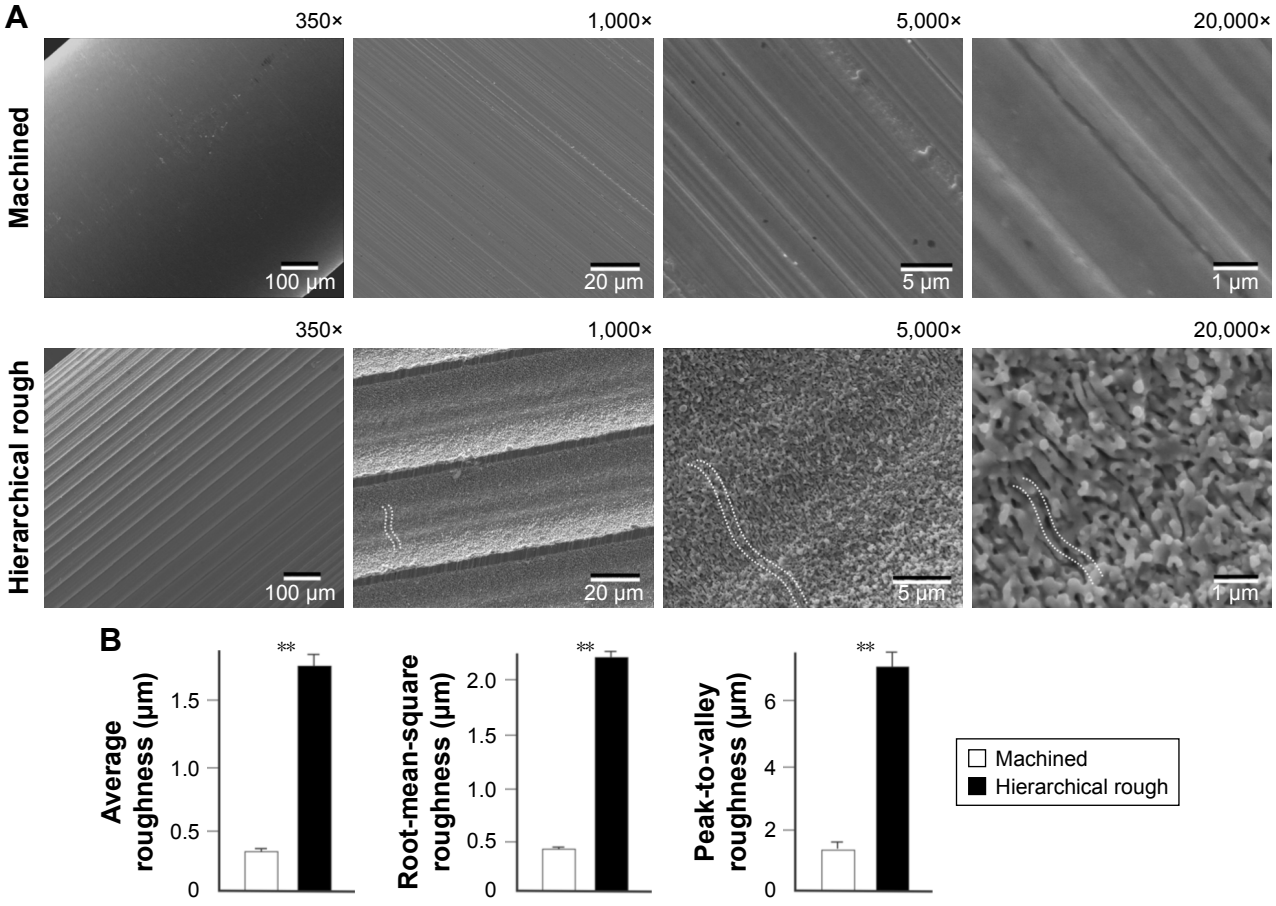

Figure 1 Creation of hierarchical rough zirconia with meso-, micro-, and nano-scale morphology.
Notes: (**A**) Scanning electron microscopic (SEM) images of machined zirconia and laser-engraved hierarchically roughened zirconia. The dotted lines within SEM images represent valley- or pit-like structures at the micron-scale. (**B**) Quantitative topographical evaluations (histograms) of the two zirconia surfaces. **$p<0.01$, statistically significant.

that were densely and evenly formed across the entire surface of the grooves (5,000× and 20,000× images, Figure 1A). The nanonodules were random in shape and direction, and the diameter was between 100 and 400 nm. The random shape and direction of nanonodules created pores and undercuts across the surface. Smaller scale valley-like waviness textures were visible at the highest magnification (dotted line in 20,000× image in Figure 1A). Collectively, these SEM findings demonstrate the creation of hierarchical roughness in zirconia consisting of meso- (groove), micro- (waviness/valley), and nano-scale (nodule) structures.

Quantitative analysis showed that the average roughness, root mean-square roughness, and peak-to-valley roughness were all significantly higher for hierarchical rough zirconia than for machined zirconia (Figure 1B).

Three-dimensional profile of zirconia surfaces

After SEM imaging, we further characterized detailed morphology of machined and hierarchical rough zirconia by 3-D profiling. First, 3-D images were taken by surface scanning at three different area sizes (Figures 2A–C, 3A–C).

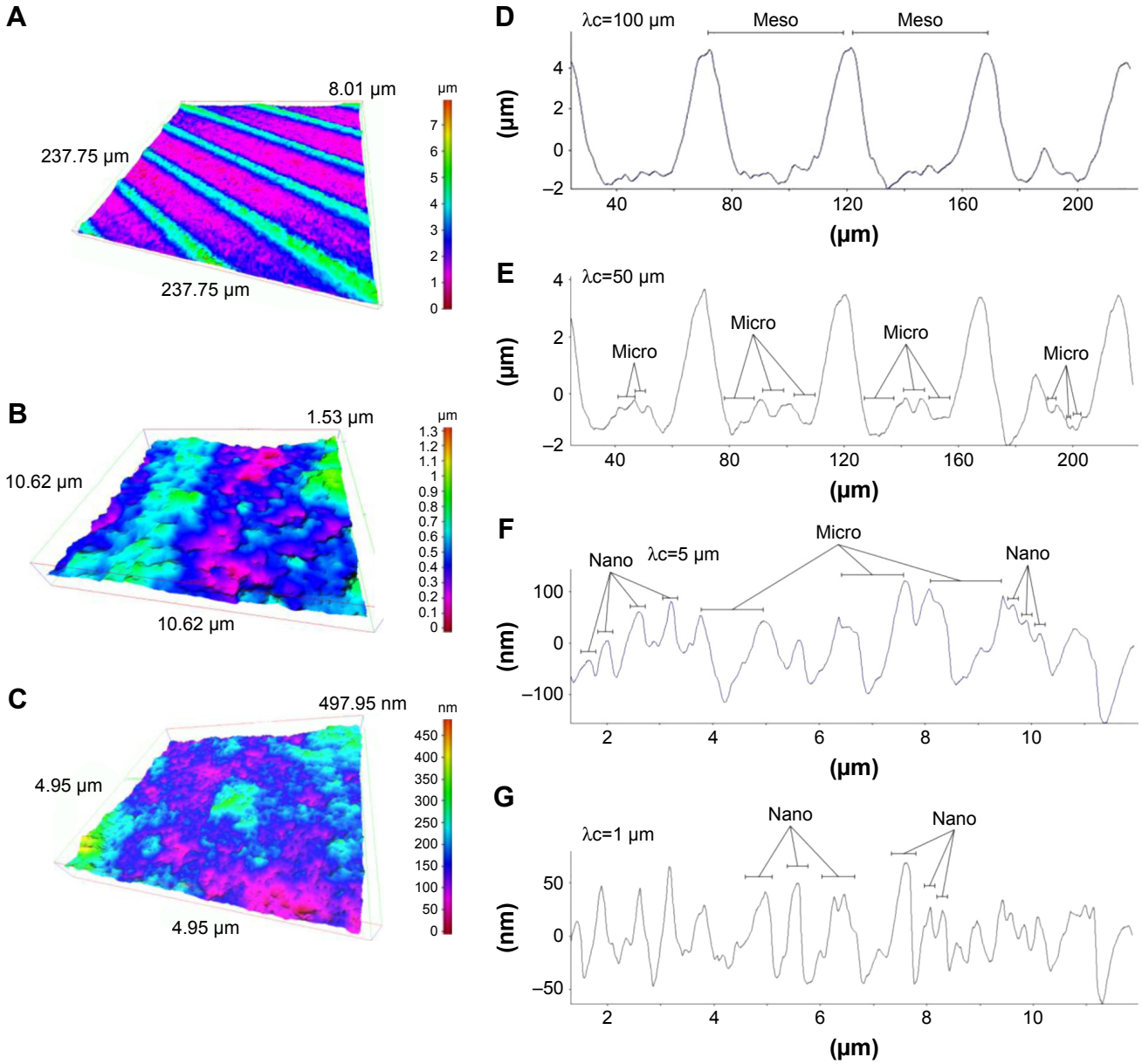

Figure 2 Three-dimensional profiles of the hierarchical rough zirconia surface.

Notes: (**A**–**C**) Three-dimensional images of the hierarchical rough zirconia surface taken with an optical profile microscope at three different magnifications. (**D**–**G**) Profile curves of the hierarchical rough zirconia surface by line scanning. Long (**D**, **E**) and short (**F**, **G**) line scanning were performed. Different filter values (cutoff value λc) were applied to draw each of the profile curves. Appearance of distinct structures at the meso-, micro-, and nano-scales are denoted within the profile curves.

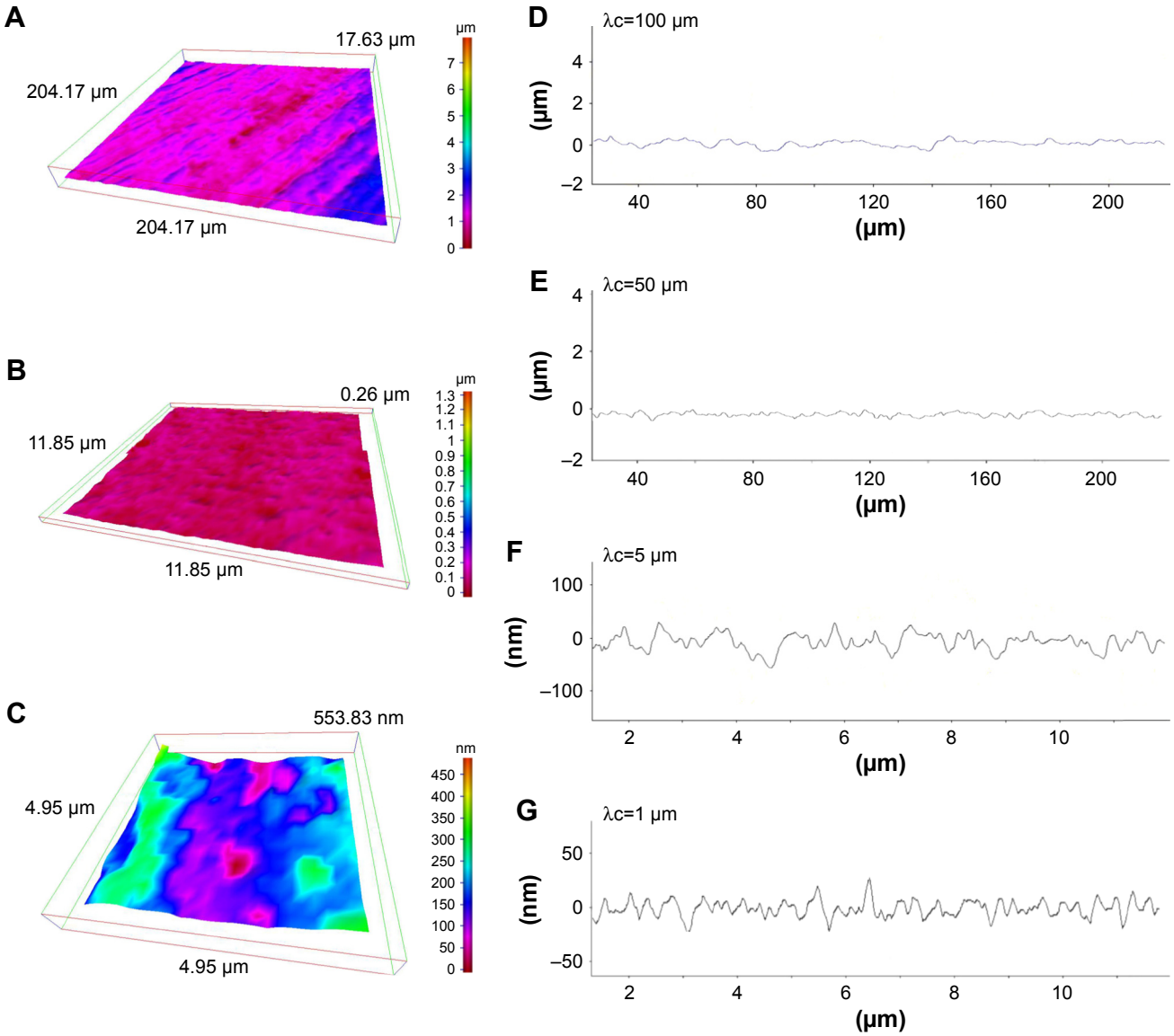

Figure 3 Three-dimensional profiles of the machined zirconia surface.

Notes: (**A**–**C**) Three-dimensional images of the machined zirconia surface taken with an optical profile microscope at three different magnifications. (**D**–**G**) Profile curves of the machined zirconia surface by line scanning. Long (**D**, **E**) and short (**F**, **G**) line scanning were performed. Different filter values (cutoff value λc) were applied to draw each of the profile curves.

The large area-scanned image confirmed the parallel formed 50 µm-width grooves on the hierarchical rough zirconia (Figure 2A), while the machined surface lacked a significant topography in this magnification, except for the machine-turned traces (Figure 3A). The mid-area scan depicted the micro-scale roughness consisting of peaks, valleys, and pits on the hierarchical rough surface (Figure 2B), whereas the machined surface had little detectable topography (Figure 3B). The small area-scan captured nano-scale roughness with protruding structures densely formed all over the hierarchical rough zirconia (Figure 2C). There was no distinct nanoscale morphological contrast on the machined surface, except for undefined microscale irregularity (Figure 3C).

We next examined the cross-sectional surface morphology of both surfaces along lines of two different lengths: a 240 µm line (Figures 2D and E, 3D and E) and a 12 µm line (Figures 2F and G, 3F and G). We also applied two different filter values (cutoff value λc) to appropriately detect the contour. The long profile curve with a high cutoff value (Figure 2D) revealed 50 µm-wide grooves of depth 6–8 µm on the hierarchical rough surface. The structures at the bottom of the groove were unclear at this cutoff value. The machined surface did not show a significant fluctuation in its curve (Figure 3D). With a low cutoff value, a distinct profile emerged that clearly demonstrated the presence of micro-scale roughness within the 50 µm-wide grooves on

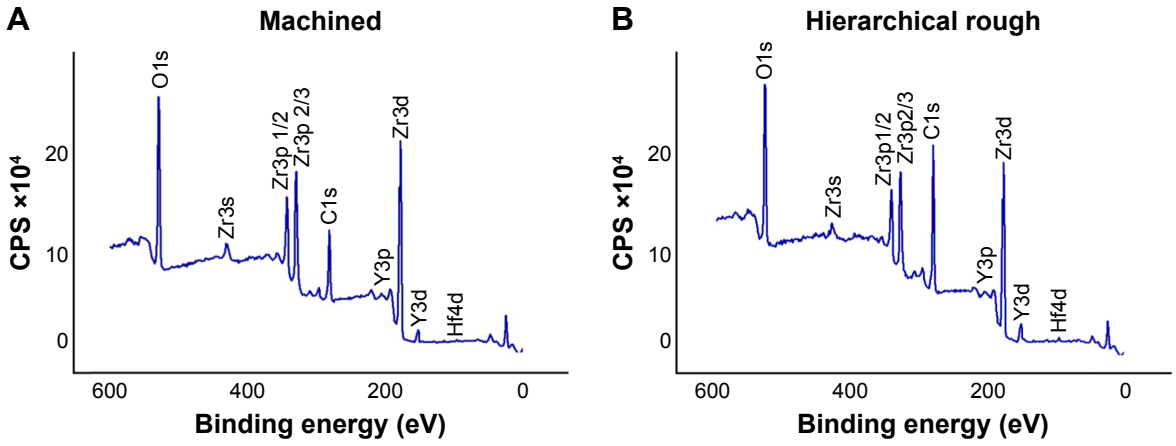

Figure 4 Chemical analysis of (**A**) machined zirconia and (**B**) hierarchical rough zirconia surfaces using x-ray photoelectron spectroscopy (XPS).
Abbreviation: CPS, counts per second.

the hierarchical rough surface (Figure 2E). The micro-scale roughness had a valley-like structure measuring up to 10 µm in width and 3 µm in depth. In contrast, the machined surface showed uniformly flat configuration under this condition of profiling (Figure 3E).

The micro-scale valleys of the hierarchical rough surface were also depicted with clearer fluctuations in the short profile curve (Figure 2F), in which there were nano-scale fluctuations simultaneously detected as protruding structures with widths up to 400 nm (Figure 2F). The machined surface show detectable irregularities at this scale (Figure 3F). With a lower cutoff value, the nano-scale fluctuations were detailed and accentuated on the hierarchical rough surface, vividly showing nodular-like peaks with widths between 10 and 400 nm and heights of approximately 10–300 nm (Figure 2G). These results corroborated the co-existence of meso-, micro-, and nano-structures on the zirconia surface seen by SEM. There was no such structure captured on the machined surface, although there were surface irregularities with a height range of 10–30 nm (Figure 3G).

Surface physicochemistry of zirconia

As show in the XPS spectra, machined and hierarchical rough zirconia surfaces both contained zirconium, yttrium, oxygen, hafnium, and carbon (Figure 4A and B). The atomic percentage of Zr3p, Y3p, O1s, and C1s were 8.14%, 0.67%, 27.94%, and 28.50%, respectively, for machined surfaces, and 5.51%, 0.88%, 21.08%, and 45.12%, for hierarchical rough surfaces. Although both machined and hierarchical rough surfaces were hydrophobic with a contact angle of H_2O being higher than 60°, the hierarchical rough surface was more hydrophobic (Figure 5).

Attachment and initial behavior of osteoblasts on zirconia

The attachment and initial behavior of osteoblasts were examined on machined and hierarchical rough zirconia surfaces. The number of osteoblasts attached to zirconia surfaces after 6 and 24 h of culture was equivalent between machined and hierarchical rough surfaces (Figure 6A). Low magnification confocal microscopy images confirmed the results and revealed a comparable number of cells on both surfaces at both 6 and 24 h incubation time-points (Figure 6B).

Magnified confocal images revealed that osteoblasts had already spread by 6 h of incubation on both surfaces (Figure 7A) and then appeared larger at 24 h on both surfaces. Although the size of cells seemed similar on both surfaces at each time point, cells on the hierarchical rough surface appeared elongated in

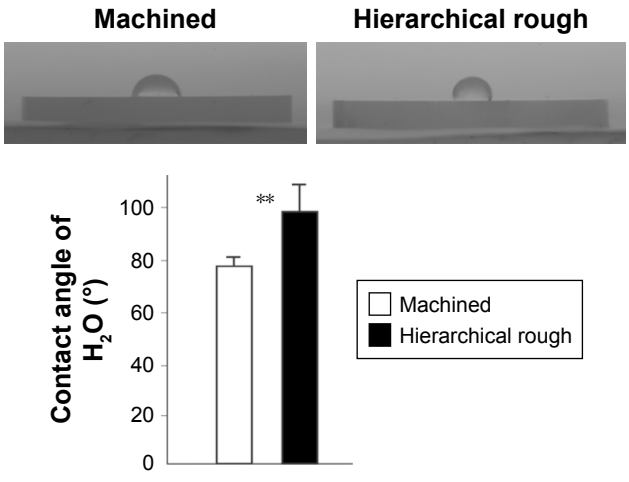

Figure 5 Hydrophilic or hydrophobic state of zirconia surfaces.
Notes: Side-view images of 10 µL double-distilled H_2O placed on zirconia disks along with the measured contact angle. **$p<0.01$, statistically significant difference between the two surfaces.

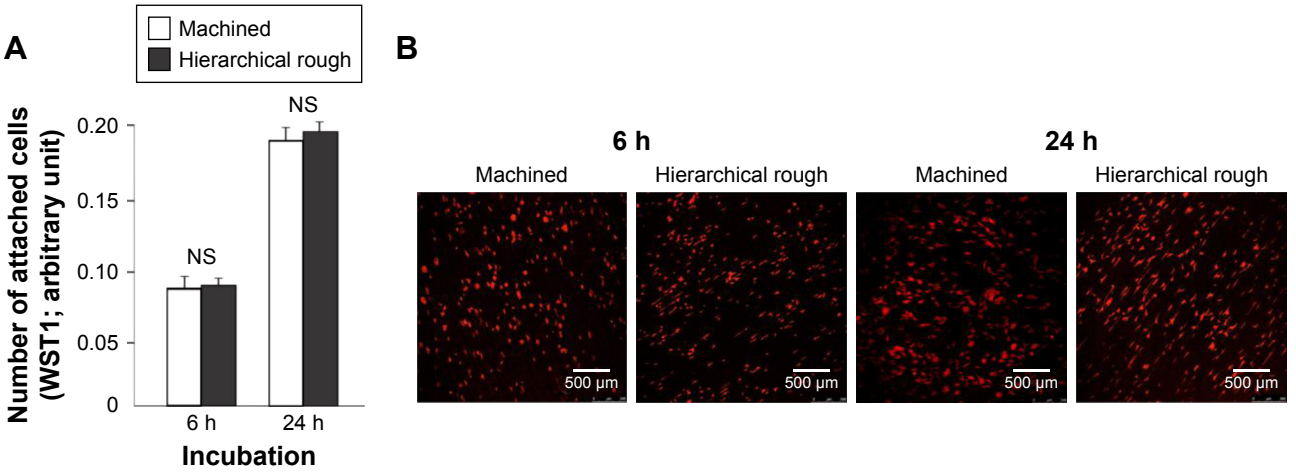

Figure 6 Attachment of osteoblasts to zirconia surfaces during the initial stage of culture.
Notes: Osteoblasts were cultured on machined and hierarchical rough zirconia surfaces. (**A**) The number of attached cells after 6 and 24 h incubations evaluated by the WST-1 assay. (**B**) Confocal microscopic images of osteoblast cultures on zirconia surfaces. NS, no statistically significant difference between the two different surfaces.

parallel with the direction of the 50 µm-wide grooves, with more advanced extension of filopodia-like cytoplasmic projections. Cytomorphometric analysis revealed that the perimeter and Feret's diameter of osteoblasts were greater on hierarchical rough surfaces than on machined surfaces, supporting the qualitative interpretation (Figure 7B).

Proliferation and functional phenotypes of osteoblasts on zirconia

The number of propagated cells and the proliferation rate evaluated by BrdU incorporation into DNA on culture day 3 were not significantly different between machined and hierarchical rough zirconia (Figure 8).

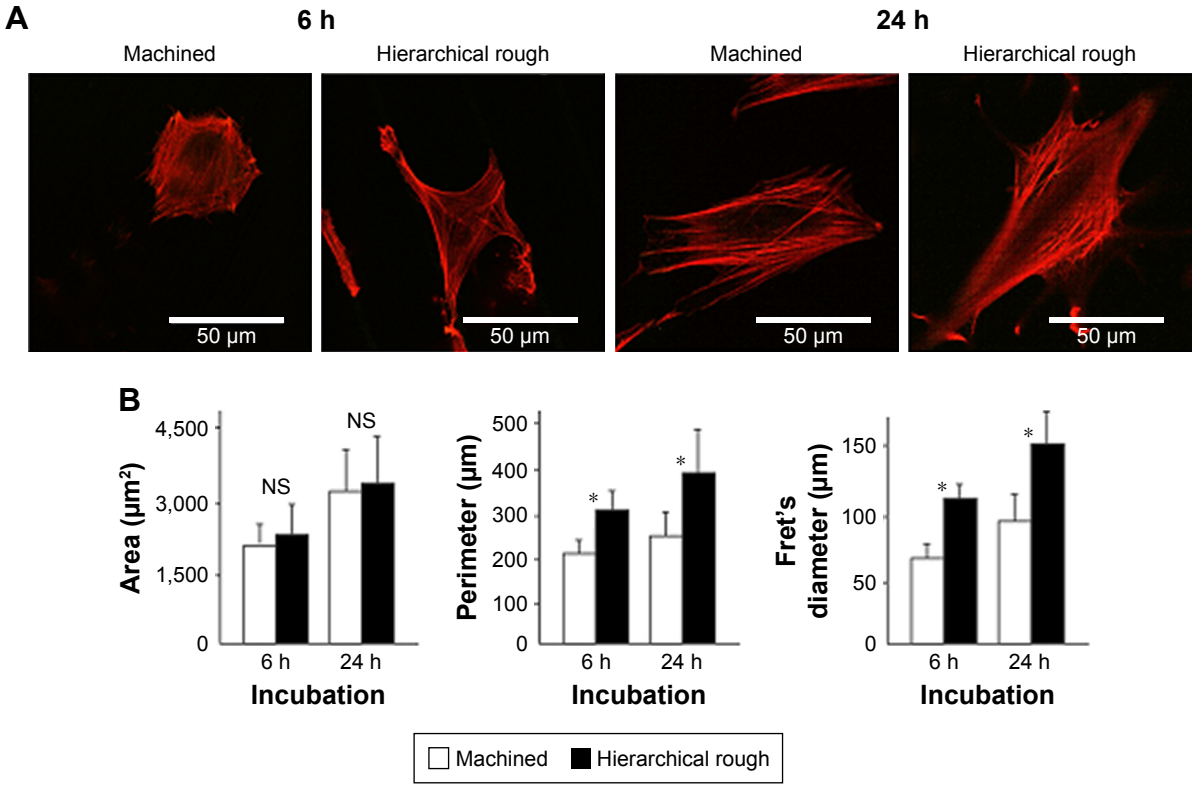

Figure 7 Spreading behavior of osteoblasts on zirconia surfaces during the initial stage of culture at 6 and 24 h after seeding.
Notes: (**A**) Confocal microscopic images of osteoblasts with immunochemical staining for cytoskeletal actin. (**B**) Histograms for cytomorphometric parameters measured from the images. *$p<0.05$, statistically significant difference between the two surfaces. NS, no statistically significant difference between the two different surfaces.

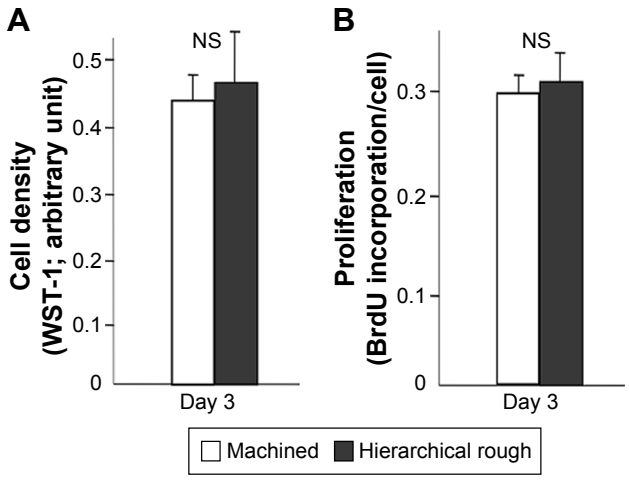

Figure 8 Proliferative activity of osteoblasts on zirconia surfaces.
Notes: (**A**) Cell density of the propagated cells evaluated on day 3 of culture using the WST-1 assay. (**B**) BrdU incorporation into DNA measured on day 3. NS, no statistically significant difference between the two different surfaces.

The ALP-positive area evaluated on day 5 was considerably larger in osteoblasts grown on hierarchical rough zirconia than on machined zirconia (Figure 9A). The expression of all bone-related genes tested was 7–25 times upregulated on hierarchical rough zirconia on day 7 (Figure 9B). The upregulation remained significant for all genes even on day 14, with particular substantial upregulation of osteopontin and osteocalcin.

Biomechanical strength of bone–implant integration

The strength of bone–implant integration evaluated by the biomechanical push-in test was 2.2-times greater for hierarchical rough zirconia implants than machined zirconia implants at week two of healing (Figure 10). The difference remained significant and undiminished at week four. Notably, the push-in value for hierarchical rough zirconia implants at week two was comparable to the push-in value for machined implants at week four.

Peri-implant tissue morphology and chemistry

Typical SEM images of machined and hierarchical rough zirconia implants after push-in testing at week two are shown in Figure 11. Nearly no tissue remnants were found on machined zirconia implant surfaces (Figure 11A), which showed the original linear trace morphology of machined zirconia (magnified images, Figure 11B and C). EDX elemental quantification (Figure 11B and C) and mapping (Figure 11D) showed little Ca or P on the machined implant surface. Instead, a significant amount of Zr was present on the machine surface (Figure 11B and C).

Hierarchical rough zirconia implants showed extensive evidence of biological tissue remnants (Figure 11E).

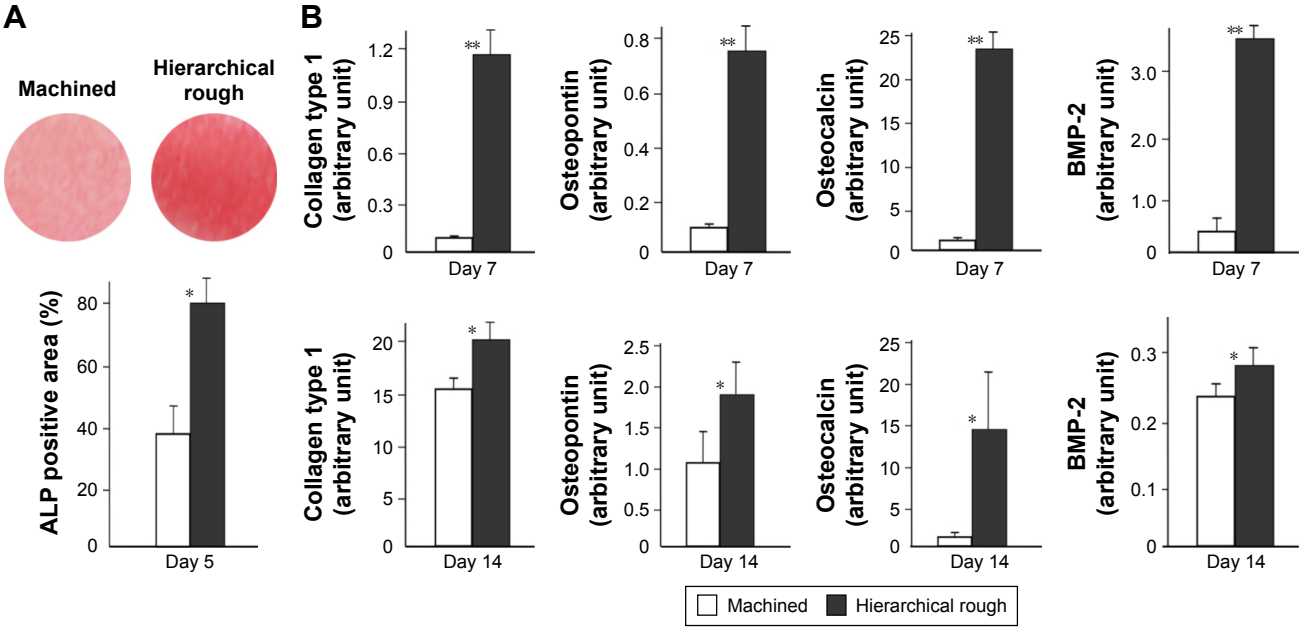

Figure 9 Functional osteoblastic differentiation on zirconia surfaces.
Notes: (**A**) Alkaline phosphatase (ALP) activity in osteoblasts on day 5 of culture. Culture images after ALP staining (top images) and ALP positive area (%) measured using those images are presented. (**B**) Results from the real-time quantitative PCR performed on days 7 and 14. *$p<0.05$, **$p<0.01$, statistically significant difference between the two surfaces.

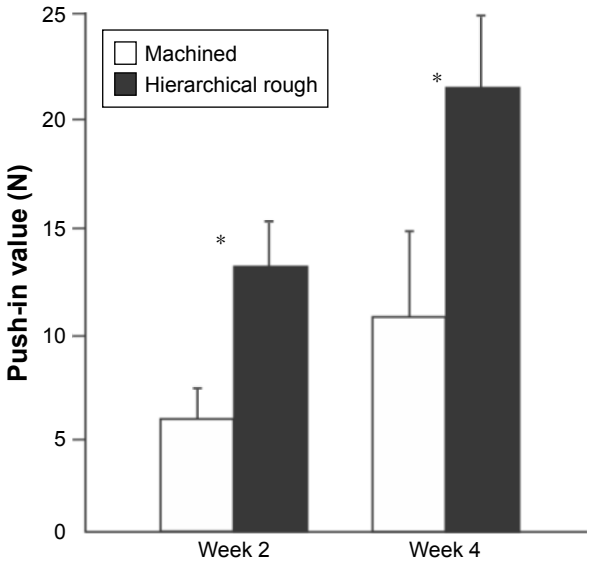

Figure 10 The strength of osseointegration evaluated by the biomechanical push-in test in the rat femur model.
Notes: *$p<0.05$; statistically significant difference between the two surfaces.

EDX analysis on the remaining tissues detected the presence of Ca and P, confirming the formation of mineralized tissue and its retention even after push-in testing (Figure 11F and G). Ca signal was clearly detected in the elemental mapping, even at the area where no obvious remaining tissue was found morphologically, indicating that thin mineralized tissue was retained at the hierarchical rough implant interface (Figure 11H).

Discussion

Here we introduced a zirconia surface with a unique roughness morphology representing the simultaneous presence of surface roughness at three hierarchical scales: meso-, micro-, and nano-scales (Figure 12). The meso-scale roughness was characterized by uniformly carved grooves of 50 µm width and 6–8 µm depth; micro-scale roughness was characterized by valleys of relatively random size and shape and width of 1–10 µm and depth of 0.1–3 µm; and nano-scale roughness consisted of densely and evenly formed nodules in random shapes and direction with widths of 10–400 nm and heights of 10–300 nm.

In vitro, hierarchical rough zirconia and machined zirconia showed a similar rate of osteoblastic proliferation, but the degree of osteoblastic differentiation was highly promoted on hierarchical zirconia, as represented by the remarkable upregulation of osteoblastic genes. In principle, the rates of osteoblastic proliferation and differentiation are inversely correlated,[66–69] meaning that when osteoblasts are robust in proliferative activity, their differentiation slows down, and vice versa. This is in part because opposing growth factors regulate osteoblastic proliferation and differentiation.[70,71]

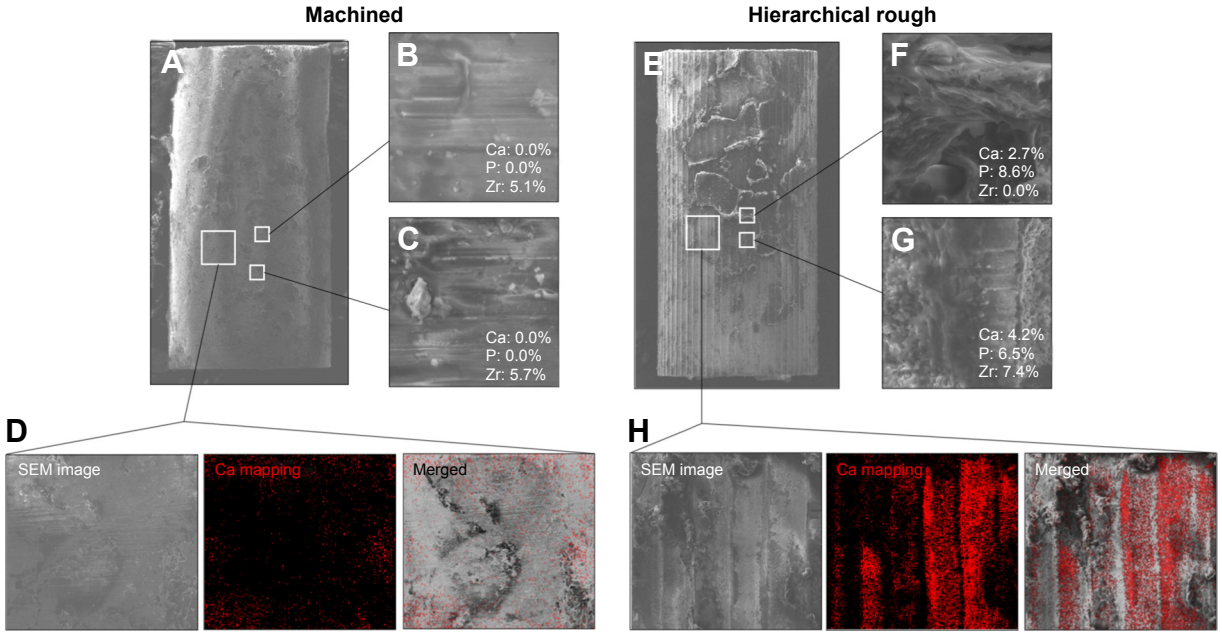

Figure 11 Peri-implant tissue morphology and chemistry around zirconia implants.
Notes: Zirconia implants with two different surfaces were retrieved after the biomechanical push-in test and analyzed by SEM and EDX. Low- and high-magnification SEM images are presented representing each of the machined (**A**–**C**) and hierarchical rough (**E**–**G**) zirconia implants. The percentage chemical composition from the EDX is presented along with the representative SEM magnified images (**B**, **C**, **F**, **G**). EDX area scans were also performed to detect Ca element as a bone ingredient (**D**, **H**).
Abbreviations: EDX, energy dispersive X-ray spectroscopy; SEM, scanning electron microscope.

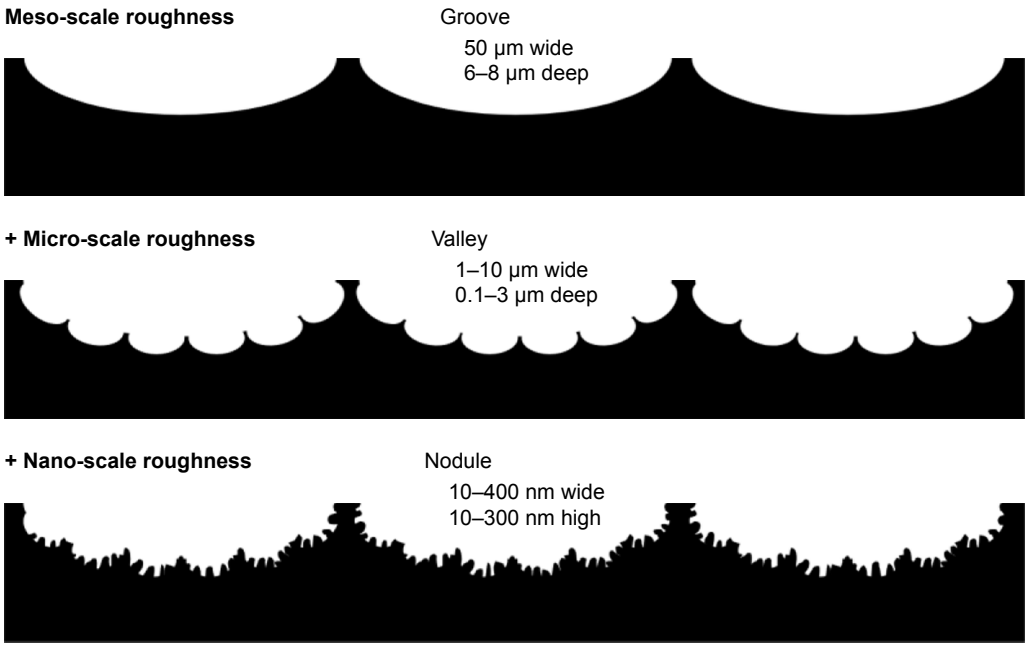

Figure 12 Schematic of the surface configuration of hierarchical rough zirconia based on the SEM analysis (Figure 1) and 3-dimensional profiling (Figure 2).
Notes: The hierarchical rough zirconia was characterized by distinct grooves, valleys, and nodules at different structural levels at the meso-, micro-, and nano-scales, respectively, as illustrated sequentially from top to bottom.

This biological dilemma also applies to osteogenic cells at biomaterial and implant surfaces. For instance, micro-roughened titanium surfaces have advantages over machined smooth surfaces in that they promote osteoblastic differentiation,[72] providing the benefit of faster bone formation.[31] The bone mass, however, is less than that around machined surfaces[72] as a result of reduced osteoblastic proliferation.[23,30,73,74] It is reported that the rate of proliferation on micro-rough titanium surfaces is one-third to one-fifth that on machined titanium surfaces.[30,73–75] It was notable that our hierarchical rough zirconia did not reduce the rate of proliferation compared to machined, smooth identical zirconia, while enabling a faster differentiation. The reason for this requires further study, but the rounded tips of the nanonodules (compared to the sharp peaks typically seen on the acid-etch-created rough titanium) might minimize a negative impact on osteoblastic proliferation. Studies on nanonodular titanium surfaces have reported osteoblastic proliferation rates similar to the present study, despite the remarkable increase in overall surface roughness.[76,77] In addition, smaller numbers of cells attach to rougher material surfaces and osteoblast spread is restricted and delayed on rougher surfaces.[75,78,79] These negative effects were not seen on hierarchical rough zirconia. On the contrary, the initial behavior of osteoblasts, ie, cell spreading, was promoted on the hierarchical rough zirconia, as shown by the increased perimeter and Feret's diameter on cytomorphometry.

Accelerating bone formation around implants is important to minimize clinical morbidity regardless of the dental or orthopedic application. This study showed that all the osteogenic genes tested were significantly upregulated on the hierarchical rough zirconia, indicating that osteoblastic differentiation was promoted. Such upregulated gene expression was seen not only at the early stages of culture on day seven but also the mid stage on day 14, suggesting that differentiation was not only expedited but also enhanced. Although the expression of early stage markers of osteoblastic differentiation such as collagen 1 were comparable between machined and hierarchical rough surfaces at day 14, the late-stage markers such as osteopontin and osteocalcin remained substantially upregulated on hierarchical rough zirconia. In our culture system, the culture starts to mineralize by day 14. Even after sufficient culture time, not all progenitor cells successfully differentiate to mature osteoblasts. The results of gene expression analysis suggest that the probability of successful osteoblastic differentiation may be increased on the hierarchical rough surface.

The strength of bone–implant integration was significantly increased for hierarchical rough zirconia both at the early healing stage at week two and the late stage at week four. This corroborated the quantitative gene expression results showing that bone-related gene expression was upregulated not only during the early stage but also the later stage of cell culture, indicating that bone–implant integration was

not just expedited but also enhanced. The strength of bone–implant integration may be the most pertinent parameter representing implant capacity as a load-bearing device, and it was enhanced by more than 100% by the hierarchical rough surface. We believe that we have developed an effective strategy to develop zirconia as an alternative material to titanium. Future studies are needed to compare the hierarchical rough zirconia with titanium with various surface types.

Enhanced bone formation around hierarchical rough zirconia was demonstrated by examining tissue morphology and chemistry around implants. More bone tissue was remnant around hierarchical rough implants after push-in test, which may explain the increased strength of bone–implant integration around these implants. Morphological and elemental analyses of implants have previously been established as a useful measure to evaluate the nature and behavior of tissues at the bone–implant interface.[65] However, the results require careful interpretation, because the method is subject to technical artifacts including tissue damage, distortion, and detachment during push-in test and sample preparation. Within these technical limitations and the qualitative nature of the examination, there was a notable difference between the two surfaces. Nearly no biological structure was found on machined surfaces, which was confirmed by little or no signals of calcium or phosphate. This represented that there was little bone tissue formed around the machined surface or bone tissue around the surface was easier to dissociate during push-in test. In contrast, a large area of hierarchical rough implants was covered with biological structures containing calcium and phosphate. In the majority of these areas, zirconia signal was completely masked. Some areas of hierarchical rough surfaces showed a positive calcium signal even without a tissue structure, indicating that a thin layer of the interfacial mineralized tissue remained after the external layer of bone was broken and detached during the push-in test. These results implied that bone formation around hierarchical rough surfaces was either greater in volume and extent, more adherent, more mineralized, or a combination of these.

In this study, we evaluated surface roughness of zirconia using a profiling algorithm based on SEM images. Theoretically, the algorithm detects surface roughness as long as it is distinctly imaged by SEM. We assume the resolution of the surface analysis was sufficient because the 3-D surface images and profiling curves clearly captured differences between machined and hierarchical rough surfaces. The quantitative roughness values also detected the differences in surface morphology. To confirm the present results and pursue further accuracy, an analysis using a contact-mode device, such as atomic force microscopy, will also be considered in future studies.

The hierarchical rough surface had a higher percentage of surface carbon than the machined surface. Natural carbon accumulation as hydrocarbons on implant materials including titanium and zirconia was recently reported[80–88] and was found to negatively impact on the ability of titanium or zirconia to attract osteoblasts and their rate of proliferation, thereby reducing bone–implant integration.[75,80,81,86,87] Further, it has been shown that decomposing and removing carbon impurities from these material surfaces by physicochemical methods such as UV light treatment effectively increases their bone–implant integration and other biological capabilities.[75,79,81,86,89–92] Despite a higher percentage of surface carbon, hierarchical rough zirconia showed a higher bone-integration capability in this study. It can be hypothesized that reducing surface carbon on hierarchical rough zirconia by UV light treatment may accentuate its biological advantage. Another influential factor may be the hydrophilic or hydrophobic state of zirconia surfaces. Although the exact mechanism is unknown and effect may be material- and cell type-dependent, hydrophilicity of material surfaces seems to have a positive effect on increasing protein adsorption and cell attachment.[75,80,86,93,94] Hydrophilic zirconia created by UV treatment attracted more osteoblasts, facilitated their spread and proliferation, and promoted bone–implant integration.[81,90,91,95] Hierarchical rough zirconia tested in the present study was more hydrophobic than machined zirconia, but it promoted cellular spread and showed a higher bone–implant integration than machined zirconia that was less hydrophobic. The effect of surface chemistry and physicochemistry, including the effect of surface carbon and other elements, hydrophilicity/hydrophobicity, and crystalline property, as well as the interaction between surface morphology and chemistry, will require further studies.

We designed rough zirconia based on the hypothesis that meso-scale (50 μm wide grooves) roughness may help increase the strength of implant anchorage by increasing bone–implant surface mechanical interlocking, while micro- and nano-scale roughness may increase implant anchorage by accelerating and enhancing bone formation. A previous study has shown that the addition of large (50–100 μm or larger) scale roughness to titanium, eg, using the titanium plasma spray technique, increases the strength of implant anchorage in bone mainly because of enhanced mechanical resistance.[96] Regarding smaller scale roughness, a number of studies have reported micro-roughness, nano-scale roughness, and their

combination promote osteoblast differentiation.[28,31,32,35,76,97–103] Indeed, here we demonstrated accelerated osteoblast differentiation on the hierarchical rough surface by revealing highly upregulated expression of several bone-related genes, strongly supporting our hypothesis and surface design strategy. It remains to be seen to what degree the 50 μm-wide grooves helped to increase implant anchorage. Now that this study has proven the feasibility of creating hierarchical rough zirconia surfaces, future studies will control each hierarchy to identify the contribution made by each structural level to ultimately optimize these parameters and create a zirconia surface with optimized biological and osseointegration capabilities.

Conclusion

We successfully created distinct hierarchical roughened morphology with meso-, micro-, and nano-scale defined structures on zirconia (Y-TZP). The hierarchical rough zirconia showed increased capability for bone–implant integration compared to machine-surfaced zirconia. This was associated with remarkably accelerated osteogenic differentiation and preserved attachment, spread, and proliferation of osteoblasts on the surface. This study provides a strategy and technology platform to produce biologically effective zirconia surface roughening for further optimization of zirconia implants.

Acknowledgment

This study has, in part, been supported by gift for research from Nantoh Co., Ltd.

Disclosure

The authors report no conflicts of interest in this work.

References

1. Hudson JI, Kenzora JE, Hebel JR, et al. Eight-year outcome associated with clinical options in the management of femoral neck fractures. *Clin Orthop Relat Res*. 1998;348:59–66.
2. Lu-Yao GL, Keller RB, Littenberg B, Wennberg JE. Outcomes after displaced fractures of the femoral neck. A meta-analysis of one hundred and six published reports. *J Bone Joint Surg Am*. 1994;76(1):15–25.
3. Tidermark J, Ponzer S, Svensson O, Söderqvist A, Törnkvist H. Internal fixation compared with total hip replacement for displaced femoral neck fractures in the elderly. A randomised, controlled trial. *J Bone Joint Surg Br*. 2003;85(3):380–388.
4. Ravikumar KJ, Marsh G. Internal fixation versus hemiarthroplasty versus total hip arthroplasty for displaced subcapital fractures of femur – 13 year results of a prospective randomised study. *Injury*. 2000;31(10):793–797.
5. Espehaug B, Furnes O, Havelin LI, Engesaeter LB, Vollset SE. The type of cement and failure of total hip replacements. *J Bone Joint Surg Br*. 2002;84(6):832–838.
6. Eskildsen SM, Wilson ZJ, McNabb DC, Olcott CW, Del Gaizo DJ. Acetabular reconstruction with the medial protrusio technique for complex primary and revision total hip arthroplasties. *J Arthroplasty*. 2017;32(11):3474–3479.
7. Baghdadi YM, Larson AN, Sierra RJ. Long-term results of the uncemented acetabular component in a primary total hip arthroplasty performed for protrusio acetabuli: a fifteen year median follow-up. *Int Orthop*. 2015;39(5):839–845.
8. Donahue GS, Lindgren V, Galea VP, Madanat R, Muratoglu OK, Malchau H. Risk factors for mid-term revision surgery in patients with articular surface replacement total hip arthroplasty. *Hip Int*. 2018;28(1):44–49.
9. Khatod M, Cafri G, Inacio MC, Schepps AL, Paxton EW, Bini SA. Revision total hip arthoplasty: factors associated with re-revision surgery. *J Bone Joint Surg Am*. 2015;97(5):359–366.
10. Salassa T, Hoeffel D, Mehle S, Tatman P, Gioe TJ. Efficacy of revision surgery for the dislocating total hip arthroplasty: report from a large community registry. *Clin Orthop Relat Res*. 2014;472(3):962–967.
11. Capon-Garcia D, Lopez-Pardo A, Alves-Perez MT. Causes for revision surgery in total hip replacement. A retrospective epidemiological analysis. *Rev Esp Cir Ortop Traumatol*. 2016;60(3):160–166.
12. Campion EW, Jette AM, Cleary PD, Harris BA. Hip fracture: a prospective study of hospital course, complications, and costs. *J Gen Intern Med*. 1987;2(2):78–82.
13. Guccione AA, Fagerson TL, Anderson JJ. Regaining functional independence in the acute care setting following hip fracture. *Phys Ther*. 1996;76(8):818–826.
14. Sugita Y, Honda Y, Kato I, Kubo K, Maeda H, Ogawa T. Role of photofunctionalization in mitigating impaired osseointegration associated with type 2 diabetes in rats. *Int J Oral Maxillofac Implants*. 2014;29(6):1293–1300.
15. Hasegawa H, Ozawa S, Hashimoto K, Takeichi T, Ogawa T. Type 2 diabetes impairs implant osseointegration capacity in rats. *Int J Oral Maxillofac Implants*. 2008;23(2):237–246.
16. Ozawa S, Ogawa T, Iida K, Sukotjo C, Hasegawa H, Nishimura RD, et al. Ovariectomy hinders the early stage of bone-implant integration: histomorphometric, biomechanical, and molecular analyses. *Bone*. 2002;30(1):137–143.
17. Moy PK, Medina D, Shetty V, Aghaloo TL. Dental implant failure rates and associated risk factors. *Int J Oral Maxillofac Implants*. 2005;20(4):569–577.
18. Klokkevold PR, Han TJ. How do smoking, diabetes, and periodontitis affect outcomes of implant treatment? *Int J Oral Maxillofac Implants*. 2007;22 Suppl:173–202.
19. Du Z, Xiao Y, Hashimi S, Hamlet SM, Ivanovski S. The effects of implant topography on osseointegration under estrogen deficiency induced osteoporotic conditions: Histomorphometric, transcriptional and ultrastructural analysis. *Acta Biomater*. 2016;42:351–363.
20. Farnsworth CW, Schott EM, Benvie AM, et al. Obesity/type 2 diabetes increases inflammation, periosteal reactive bone formation, and osteolysis during *Staphylococcus aureus* implant-associated bone infection. *J Orthop Res*. Epub 2017 Dec 11.
21. Monje A, Catena A, Borgnakke WS. Association between diabetes mellitus/hyperglycaemia and peri-implant diseases: Systematic review and meta-analysis. *J Clin Periodontol*. 2017;44(6):636–648.
22. Annibali S, Pranno N, Cristalli MP, La Monaca G, Polimeni A. Survival analysis of implant in patients with diabetes mellitus: a systematic review. *Implant Dent*. 2016;25(5):663–674.
23. Bachle M, Kohal RJ. A systematic review of the influence of different titanium surfaces on proliferation, differentiation and protein synthesis of osteoblast-like MG63 cells. *Clin Oral Implants Res*. 2004;15(6):683–692.
24. Boyan BD, Hummert TW, Dean DD, Schwartz Z. Role of material surfaces in regulating bone and cartilage cell response. *Biomaterials*. 1996;17(2):137–146.
25. Kieswetter K, Schwartz Z, Dean DD, Boyan BD. The role of implant surface characteristics in the healing of bone. *Crit Rev Oral Biol Med*. 1996;7(4):329–345.
26. Shalabi MM, Gortemaker A, Van't Hof MA, Jansen JA, Creugers NH. Implant surface roughness and bone healing: a systematic review. *J Dent Res*. 2006;85(6):496–500.

27. Cooper LF. A role for surface topography in creating and maintaining bone at titanium endosseous implants. *J Prosthet Dent*. 2000;84(5):522–534.
28. Mendonca G, Mendonca DB, Aragao FJ, Cooper LF. Advancing dental implant surface technology – From micron- to nanotopography. *Biomaterials*. 2008;29(28):3822–3835.
29. Cooper LF, Masuda T, Yliheikkila PK, Felton DA. Generalizations regarding the process and phenomenon of osseointegration. Part II. In vitro studies. *Int J Oral Maxillofac Implants*. 1998;13(2):163–174.
30. Takeuchi K, Saruwatari L, Nakamura HK, Yang JM, Ogawa T. Enhanced intrinsic biomechanical properties of osteoblastic mineralized tissue on roughened titanium surface. *J Biomed Mater Res A*. 2005;72(3):296–305.
31. Ogawa T, Nishimura I. Different bone integration profiles of turned and acid-etched implants associated with modulated expression of extracellular matrix genes. *Int J Oral Maxillofac Implants*. 2003;18(2):200–210.
32. Ogawa T, Nishimura I. Genes differentially expressed in titanium implant healing. *J Dent Res*. 2006;85(6):566–570.
33. Butz F, Aita H, Wang CJ, Ogawa T. Harder and stiffer bone osseointegrated to roughened titanium. *J Dent Res*. 2006;85(6):560–565.
34. Nakamura H, Shim J, Butz F, Aita H, Gupta V, Ogawa T. Glycosaminoglycan degradation reduces mineralized tissue-titanium interfacial strength. *J Biomed Mater Res A*. 2006;77(3):478–486.
35. Masuda T, Yliheikkila PK, Felton DA, Cooper LF. Generalizations regarding the process and phenomenon of osseointegration. Part I. In vivo studies. *Int J Oral Maxillofac Implants*. 1998;13(1):17–29.
36. Albrektsson T, Wennerberg A. Oral implant surfaces: Part 2 – review focusing on clinical knowledge of different surfaces. *Int J Prosthodont*. 2004;17(5):544–564.
37. Brunski JB, Puleo DA, Nanci A. Biomaterials and biomechanics of oral and maxillofacial implants: current status and future developments. *Int J Oral Maxillofac Implants*. 2000;15(1):15–46.
38. Manzano G, Herrero LR, Montero J. Comparison of clinical performance of zirconia implants and titanium implants in animal models: a systematic review. *Int J Oral Maxillofac Implants*. 2014;29(2):311–320.
39. Elnayef B, Lazaro A, Suarez-Lopez Del Amo F, et al. Zirconia implants as an alternative to titanium: a systematic review and meta-analysis. *Int J Oral Maxillofac Implants*. 2017;32(3):e125–e134.
40. Hashim D, Cionca N, Courvoisier DS, Mombelli A. A systematic review of the clinical survival of zirconia implants. *Clin Oral Investig*. 2016;20(7):1403–1417.
41. Wenz HJ, Bartsch J, Wolfart S, Kern M. Osseointegration and clinical success of zirconia dental implants: a systematic review. *Int J Prosthodont*. 2008;21(1):27–36.
42. Weingart D, Steinemann S, Schilli W, et al. Titanium deposition in regional lymph nodes after insertion of titanium screw implants in maxillofacial region. *Int J Oral Maxillofac Surg*. 1994;23(6 Pt 2):450–452.
43. Bianco PD, Ducheyne P, Cuckler JM. Local accumulation of titanium released from a titanium implant in the absence of wear. *J Biomed Mater Res*. 1996;31(2):227–234.
44. Frisken KW, Dandie GW, Lugowski S, Jordan G. A study of titanium release into body organs following the insertion of single threaded screw implants into the mandibles of sheep. *Aust Dent J*. 2002;47(3):214–217.
45. Sicilia A, Cuesta S, Coma G, et al. Titanium allergy in dental implant patients: a clinical study on 1500 consecutive patients. *Clin Oral Implants Res*. 2008;19(8):823–835.
46. Roehling S, Astasov-Frauenhoffer M, Hauser-Gerspach I, et al. In vitro biofilm formation on titanium and zirconia implant surfaces. *J Periodontol*. 2017;88(3):298–307.
47. Al-Radha AS, Dymock D, Younes C, O'Sullivan D. Surface properties of titanium and zirconia dental implant materials and their effect on bacterial adhesion. *J Dent*. 2012;40(2):146–153.
48. Nakamura K, Kanno T, Milleding P, Ortengren U. Zirconia as a dental implant abutment material: a systematic review. *Int J Prosthodont*. 2010;23(4):299–309.
49. Egawa M, Miura T, Kato T, Saito A, Yoshinari M. In vitro adherence of periodontopathic bacteria to zirconia and titanium surfaces. *Dent Mater J*. 2013;32(1):101–106.
50. Rimondini L, Cerroni L, Carrassi A, Torricelli P. Bacterial colonization of zirconia ceramic surfaces: an in vitro and in vivo study. *Int J Oral Maxillofac Implants*. 2002;17(6):793–798.
51. Scarano A, Di Carlo F, Quaranta M, Piattelli A. Bone response to zirconia ceramic implants: an experimental study in rabbits. *J Oral Implantol*. 2003;29(1):8–12.
52. Kohal RJ, Klaus G. A zirconia implant-crown system: a case report. *Int J Periodontics Restorative Dent*. 2004;24(2):147–153.
53. Al Qahtani WM, Schille C, Spintzyk S, et al. Effect of surface modification of zirconia on cell adhesion, metabolic activity and proliferation of human osteoblasts. *Biomed Tech (Berl)*. 2017;62(1):75–87.
54. Hoffmann O, Angelov N, Zafiropoulos GG, Andreana S. Osseointegration of zirconia implants with different surface characteristics: an evaluation in rabbits. *Int J Oral Maxillofac Implants*. 2012;27(2):352–358.
55. Bormann KH, Gellrich NC, Kniha H, Dard M, Wieland M, Gahlert M. Biomechanical evaluation of a microstructured zirconia implant by a removal torque comparison with a standard Ti-SLA implant. *Clin Oral Implants Res*. 2012;23(10):1210–1216.
56. Altmann B, Rabel K, Kohal RJ, et al. Cellular transcriptional response to zirconia-based implant materials. *Dent Mater*. 2017;33(2):241–255.
57. Camposilvan E, Flamant Q, Anglada M. Surface roughened zirconia: towards hydrothermal stability. *J Mech Behav Biomed Mater*. 2015;47:95–106.
58. Rocchietta I, Fontana F, Addis A, Schupbach P, Simion M. Surface-modified zirconia implants: tissue response in rabbits. *Clin Oral Implants Res*. 2009;20(8):844–850.
59. Montero J, Bravo M, Guadilla Y, et al. Comparison of clinical and histologic outcomes of zirconia versus titanium implants placed in fresh sockets: a 5-month study in beagles. *Int J Oral Maxillofac Implants*. Epub 2015 Feb 11.
60. Kohal RJ, Bachle M, Att W, et al. Osteoblast and bone tissue response to surface modified zirconia and titanium implant materials. *Dent Mater*. 2013;29(7):763–776.
61. Gahlert M, Gudehus T, Eichhorn S, Steinhauser E, Kniha H, Erhardt W. Biomechanical and histomorphometric comparison between zirconia implants with varying surface textures and a titanium implant in the maxilla of miniature pigs. *Clin Oral Implants Res*. 2007;18(5):662–668.
62. Schliephake H, Hefti T, Schlottig F, Gedet P, Staedt H. Mechanical anchorage and peri-implant bone formation of surface-modified zirconia in minipigs. *J Clin Periodontol*. 2010;37(9):818–828.
63. Depprich R, Zipprich H, Ommerborn M, et al. Osseointegration of zirconia implants compared with titanium: an in vivo study. *Head Face Med*. 2008;4:30.
64. Mihatovic I, Golubovic V, Becker J, Schwarz F. Bone tissue response to experimental zirconia implants. *Clin Oral Investig*. 2017;21(2):523–532.
65. Ogawa T, Ozawa S, Shih JH, et al. Biomechanical evaluation of osseous implants having different surface topographies in rats. *J Dent Res*. 2000;79(11):1857–1863.
66. Stein GS, Lian JB. Molecular mechanisms mediating proliferation/differentiation interrelationships during progressive development of the osteoblast phenotype. *Endocr Rev*. 1993;14(4):424–442.
67. Siddhanti SR, Quarles LD. Molecular to pharmacologic control of osteoblast proliferation and differentiation. *J Cell Biochem*. 1994;55(3):310–320.
68. Alborzi A, Mac K, Glackin CA, Murray SS, Zernik JH. Endochondral and intramembranous fetal bone development: osteoblastic cell proliferation, and expression of alkaline phosphatase, m-twist, and histone H4. *J Craniofac Genet Dev Biol*. 1996;16(2):94–106.
69. Owen TA, Aronow M, Shalhoub V, et al. Progressive development of the rat osteoblast phenotype in vitro: reciprocal relationships in expression of genes associated with osteoblast proliferation and differentiation during formation of the bone extracellular matrix. *J Cell Physiol*. 1990;143(3):420–430.

70. Spinella-Jaegle S, Roman-Roman S, Faucheu C, et al. Opposite effects of bone morphogenetic protein-2 and transforming growth factor-beta1 on osteoblast differentiation. *Bone*. 2001;29(4):323–330.
71. Alliston T, Choy L, Ducy P, Karsenty G, Derynck R. TGF-beta-induced repression of CBFA1 by Smad3 decreases cbfa1 and osteocalcin expression and inhibits osteoblast differentiation. *Embo J*. 2001;20(9):2254–2272.
72. Ogawa T, Sukotjo C, Nishimura I. Modulated bone matrix-related gene expression is associated with differences in interfacial strength of different implant surface roughness. *J Prosthodont*. 2002;11(4):241–247.
73. Zhao G, Schwartz Z, Wieland M, et al. High surface energy enhances cell response to titanium substrate microstructure. *J Biomed Mater Res A*. 2005;74(1):49–58.
74. Boyan BD, Bonewald LF, Paschalis EP, et al. Osteoblast-mediated mineral deposition in culture is dependent on surface microtopography. *Calcif Tissue Int*. 2002;71(6):519–529.
75. Aita H, Hori N, Takeuchi M, et al. The effect of ultraviolet functionalization of titanium on integration with bone. *Biomaterials*. 2009;30(6):1015–1025.
76. Kubo K, Tsukimura N, Iwasa F, et al. Cellular behavior on TiO2 nanonodular structures in a micro-to-nanoscale hierarchy model. *Biomaterials*. 2009;30(29):5319–5329.
77. Tsukimura N, Yamada M, Iwasa F, et al. Synergistic effects of UV photofunctionalization and micro-nano hybrid topography on the biological properties of titanium. *Biomaterials*. 2011;32(19):4358–4368.
78. Iwasa F, Hori N, Ueno T, Minamikawa H, Yamada M, Ogawa T. Enhancement of osteoblast adhesion to UV-photofunctionalized titanium via an electrostatic mechanism. *Biomaterials*. 2010;31(10):2717–2727.
79. Ueno T, Ikeda T, Tsukimura N, et al. Novel antioxidant capability of titanium induced by UV light treatment. *Biomaterials*. 2016;108:177–186.
80. Att W, Hori N, Takeuchi M, et al. Time-dependent degradation of titanium osteoconductivity: an implication of biological aging of implant materials. *Biomaterials*. 2009;30(29):5352–5363.
81. Att W, Takeuchi M, Suzuki T, Kubo K, Anpo M, Ogawa T. Enhanced osteoblast function on ultraviolet light-treated zirconia. *Biomaterials*. 2009;30(7):1273–1280.
82. Minamikawa H, Att W, Ikeda T, Hirota M, Ogawa T. Long-term progressive degradation of the biological capability of titanium. *Materials*. 2016;9:E102.
83. Hori N, Att W, Ueno T, et al. Age-dependent degradation of the protein adsorption capacity of titanium. *J Dent Res*. 2009;88(7):663–667.
84. Lee JH, Ogawa T. The biological aging of titanium implants. *Implant Dent*. 2012;21(5):415–421.
85. Ogawa T. Ultraviolet photofunctionalization of titanium implants. *Oral Craniofac Tissue Eng*. 2012;2:151–158.
86. Att W, Hori N, Iwasa F, Yamada M, Ueno T, Ogawa T. The effect of UV-photofunctionalization on the time-related bioactivity of titanium and chromium-cobalt alloys. *Biomaterials*. 2009;30(26):4268–4276.
87. Iwasa F, Tsukimura N, Sugita Y, et al. TiO2 micro-nano-hybrid surface to alleviate biological aging of UV-photofunctionalized titanium. *Int J Nanomed*. 2011;6:1327–1341.
88. Att W, Ogawa T. Biological aging of implant surfaces and their restoration with ultraviolet light treatment: a novel understanding of osseointegration. *Int J Oral Maxillofac Implants*. 2012;27(4):753–761.
89. Ueno T, Takeuchi M, Hori N, et al. Gamma ray treatment enhances bioactivity and osseointegration capability of titanium. *J Biomed Mater Res B Appl Biomater*. 2012;100(8):2279–2287.
90. Altmann B, Kohal RJ, Steinberg T, et al. Distinct cell functions of osteoblasts on UV-functionalized titanium- and zirconia-based implant materials are modulated by surface topography. *Tissue Eng Part C Methods*. 2013;19(11):850–863.
91. Tuna T, Wein M, Altmann B, Steinberg T, Fischer J, Att W. Effect of ultraviolet photofunctionalisation on the cell attractiveness of zirconia implant materials. *Eur Cell Mater*. 2015;29:82–94; discussion 95–96.
92. Tuna T, Wein M, Swain M, Fischer J, Att W. Influence of ultraviolet photofunctionalization on the surface characteristics of zirconia-based dental implant materials. *Dent Mater*. 2015;31(2):e14–e24.
93. Iwasa F, Baba K, Ogawa T. Enhanced intracellular signaling pathway in osteoblasts on ultraviolet lighttreated hydrophilic titanium. *Biomed Res*. 2016;37(1):1–11.
94. Ikeda T, Hagiwara Y, Hirota M, et al. Effect of photofunctionalization on fluoride-treated nanofeatured titanium. *J Biomater Appl*. 2014;28(8):1200–1212.
95. Brezavscek M, Fawzy A, Bachle M, Tuna T, Fischer J, Att W. The effect of UV treatment on the osteoconductive capacity of zirconia-based materials. *Materials (Basel)*. 2016;9(12):E958.
96. Klokkevold PR, Johnson P, Dadgostari S, Caputo A, Davies JE, Nishimura RD. Early endosseous integration enhanced by dual acid etching of titanium: a torque removal study in the rabbit. *Clin Oral Implants Res*. 2001;12(4):350–357.
97. Cooper LF, Zhou Y, Takebe J, et al. Fluoride modification effects on osteoblast behavior and bone formation at TiO2 grit-blasted c.p. titanium endosseous implants. *Biomaterials*. 2006;27(6):926–936.
98. Guo J, Padilla RJ, Ambrose W, De Kok IJ, Cooper LF. The effect of hydrofluoric acid treatment of TiO2 grit blasted titanium implants on adherent osteoblast gene expression in vitro and in vivo. *Biomaterials*. 2007;28(36):5418–5425.
99. Albrektsson T, Wennerberg A. Oral implant surfaces: Part 1 – review focusing on topographic and chemical properties of different surfaces and in vivo responses to them. *Int J Prosthodont*. 2004;17(5):536–543.
100. Wennerberg A, Albrektsson T. Effects of titanium surface topography on bone integration: a systematic review. *Clin Oral Implants Res*. 2009;20 Suppl 4:172–184.
101. Wennerberg A, Albrektsson T. On implant surfaces: a review of current knowledge and opinions. *Int J Oral Maxillofac Implants*. 2010;25(1):63–74.
102. Ogawa T, Saruwatari L, Takeuchi K, Aita H, Ohno N. Ti Nano-nodular Structuring for Bone Integration and Regeneration. *J Dent Res*. 2008;87(8):751–756.
103. Nishimura I, Huang Y, Butz F, Ogawa T, Lin A, Wang CJ. Discrete deposition of hydroxyapatite nanoparticles on a titanium implant with predisposing substrate microtopography accelerated osseointegration. *Nanotechnology*. 2007;18(24):245101.